by positive staining with several monoclonal antibodies, i.e., RM-4 (Cosmo Bio Co., Ltd.) for macrophages, MRC OX-8 (mouse anti-rat CD8 alpha mAb, Serotec) for nonhelper T cells, and MRC OX-35 (mouse anti-rat CD4 mAb, Serotec) for helper T cells. The epithelioid cells and macrophages found around epithelioid cell granulomas were determined by positive staining with RM-4 (Fig. 2c). T cell subsets were characterized using MRC OX-35 and MRC OX-8.

The formalin-fixed, paraffin-embedded tumor and granuloma tissues were sectioned at 3 μm thickness and stained with hematoxylin and eosin (HE), whereas the frozen granuloma tissues were cut at 4 μm thickness. Immunohistochemical staining was carried out according to a standard immunostaining procedure [7–9]. Briefly, after deparaffization and rehydration (for MRC OX-6, MRC OX-8, and RM-4 mAbs), tissue sections were heated at 121°C for 15 min in 10 mM sodium citrate buffer, pH 6.0, for antigen retrieval (MRC OX-6 mAb). Frozen sections were fixed in ethanol (for MRC OX-3, MRC OX-17, and MRC OX-35 mAbs). Endogenous peroxidase activity was blocked for 5 min in methanol containing 3% hydrogen peroxide. Thereafter, slides were incubated with primary antibodies for 30 min at room temperature. The bound antibody was visualized by the avidin/biotin conjugate immunoperoxidase procedure using the HISTOFINE SAB 2 system HRP (Dako, Japan) and 3,3′-diaminobenzidine tetrahydrochloride (DAB) (Dako, Japan). Counterstaining was performed with hematoxylin.

PET imaging

PET experiments were performed in rats bearing BCG granulomas or KDH-8 tumors before (control) and after a prednisolone treatment. Eighteen days after BCG inoculation or 13 days after KDH-8 inoculation, the rats (n=3 for BCG granulomas and KDH-8 tumors, respectively) were fasted overnight, and anesthetized with pentobarbital (50 mg/kg body weight, i.p.). The rats were placed in a PET scanner (SHR-7700L, Hamamatsu Photonics, Hamamatsu, Japan) in a supine position and injected with FDG (28–30 MBq/rat) in the lateral tail vein. Sixty minutes after the injection of FDG, the rats underwent a first PET scanning for 15 min. After the PET scanning, the rats were treated with methylprednisolone acetate (8 mg/kg body weight). Twenty hours after the prednisolone treatment, a second FDG-PET scan was carried out using the same procedures as the first PET scan. The PET images were reconstructed by a standard filtered back-projection using a Hamming filter into a $256 \times 256 \times 31$ ($0.6 \times 0.6 \times 3.6$ mm) matrix. The spatial resolution of the reconstructed images was 2.7 mm in the plane [10].

Statistical analysis

All values are expressed as mean ± standard deviation. To evaluate the significance of the differences in the values obtained between the control group and the treated group, an unpaired student's t test was performed.

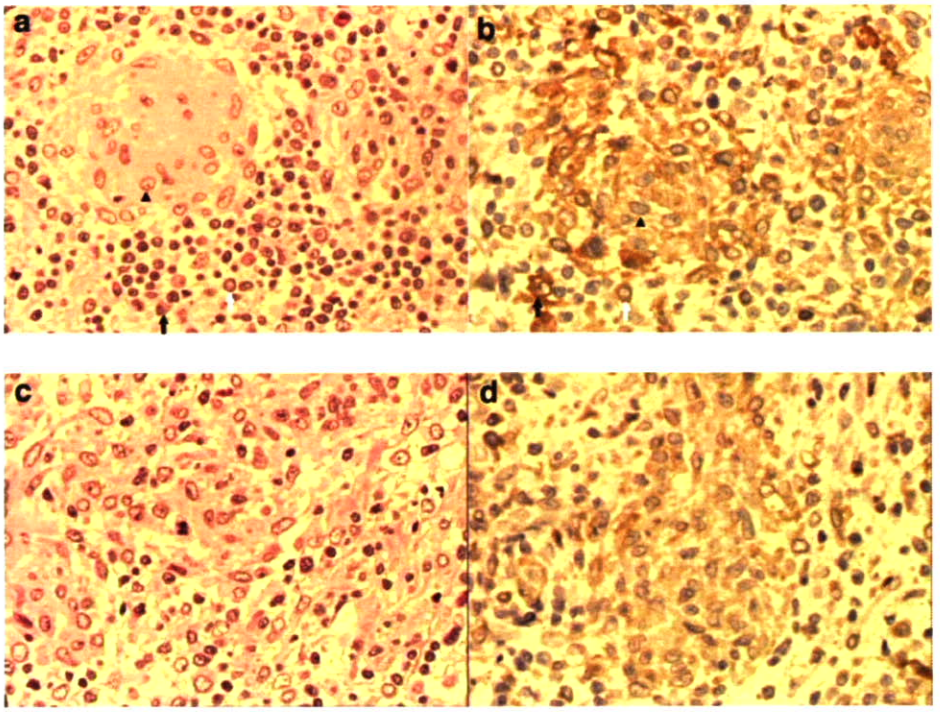

Fig. 1 Microscopic images (x 400) of HE-stained (**a**, **c**) and immunostained granuloma (**b**, **d**) for Ia antigen with MRC OX-6 mAb in control (**a**, **b**) and pretreated rats (**c**, **d**). **a** Mature epithelioid cell granuloma-formation and massive lymphocyte-infiltration. **b** Infiltrations of Ia-positive epithelioid cells and macrophages in granuloma and Ia-positive lymphocytes in granuloma periphery (for MRC OX-6). **c** Reduction of epithelioid cell granuloma-formation and lymphocyte-infiltration. **d** Reduction of infiltrations of Ia+ macrophages and Ia+ lymphocytes around granuloma. *Black arrow head* indicates epithelioid cell granuloma; *black arrow*, macrophage infiltration; *white arrow*, lymphocyte infiltration

A two-tailed value of $P<0.05$ was considered significant. The statistical program Stat View 5.0 was used for the data assessment.

Results

Histopathological findings

In the control animals inoculated with BCG, mature epithelioid cell granuloma-formation and massive lymphocyte-infiltration were observed in the calf muscle (Fig. 1a). Immunohistochemical staining with the MRC OX-6 mAb showed the accumulation of Ia^+ macrophages and Ia^+ lymphocytes into the periphery of the granuloma (Fig. 1b). In the prednisolone pretreatment group, reduction in the levels of epithelioid cell granuloma-formation and lymphocyte-infiltration and in the levels of Ia^+ macrophage-infiltration and Ia^+ lymphocyte-infiltration were observed (Fig. 1c and d). Immunostaining with MRC OX-3 and MRC OX-17 mAbs also showed the accumulation of Ia+ macrophages and Ia+ lymphocytes into the periphery of the granulomas in the control animals (Fig. 2a and b).

The different cell types in the granulomatous tissues were characterized by positive staining with several monoclonal antibodies. The epithelioid cells and macrophages determined by positive staining with RM-4 were found in the epithelioid cell granulomas and around epithelioid cell granulomas (Fig. 2c). Immunohistochemical staining of CD4 and CD8 showed numerous CD4+ (helper T cells) and CD8+ T cells (nonhelper T cells) surrounding the granulomas (Fig. 2d and e).

In the control animals inoculated with KDH-8, massive viable and proliferating cancer cells were observed by HE staining (Fig. 3a). Immunohistochemical staining with the MRC OX-6 mAb showed scattered Ia^+ macrophages-infiltration and Ia^+ lymphocytes-infiltration into the viable tumor cells (Fig. 3b). There were no histopathological changes for tumor tissue after treatment with prednisolone (Fig. 3c and d).

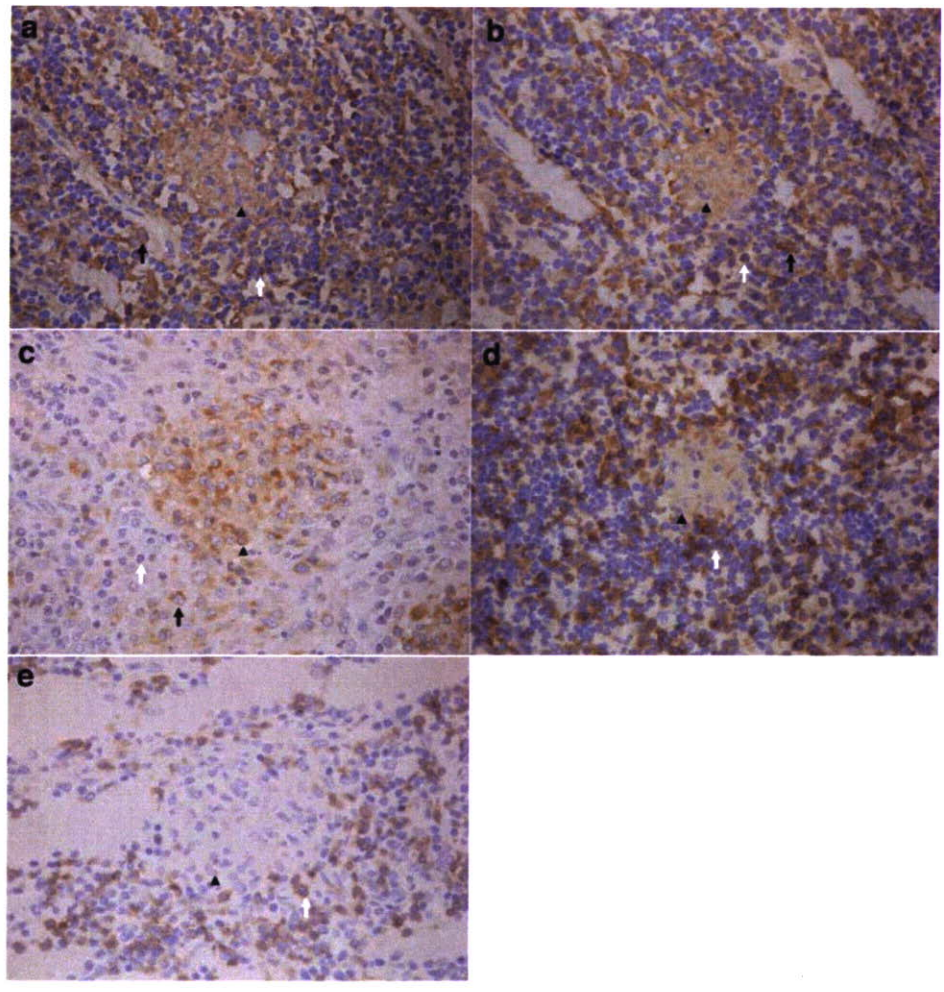

Fig. 2 Microscopic images (x 400) of immunostained for Ia antigen with MRC OX-3 (**a**), MRC OX-17 mAbs (**b**), and cell type characterization (**c**-**e**) in granulomas of control rats. **a** Accumulation of Ia+ epithelioid cells, Ia+ macrophages and Ia+ lymphocytes were characterized by MRC OX-3 mAb. **b** Accumulation of Ia+ epithelioid cells, Ia+ macrophages, and Ia+ lymphocytes were characterized by MRC OX-17 mAb. **c** The epithelioid cells and macrophages were determined by RM-4 positive staining. **d** CD4+ T cells (helper T cells) were determined by MRC OX-35 mAb. **e** CD8+ T cells (nonhelper T cells) were determined by MRC OX-8 mAb. *Black arrow head* indicates epithelioid cell granuloma; *black arrow*, macrophage infiltration; *white arrow*, lymphocyte infiltration

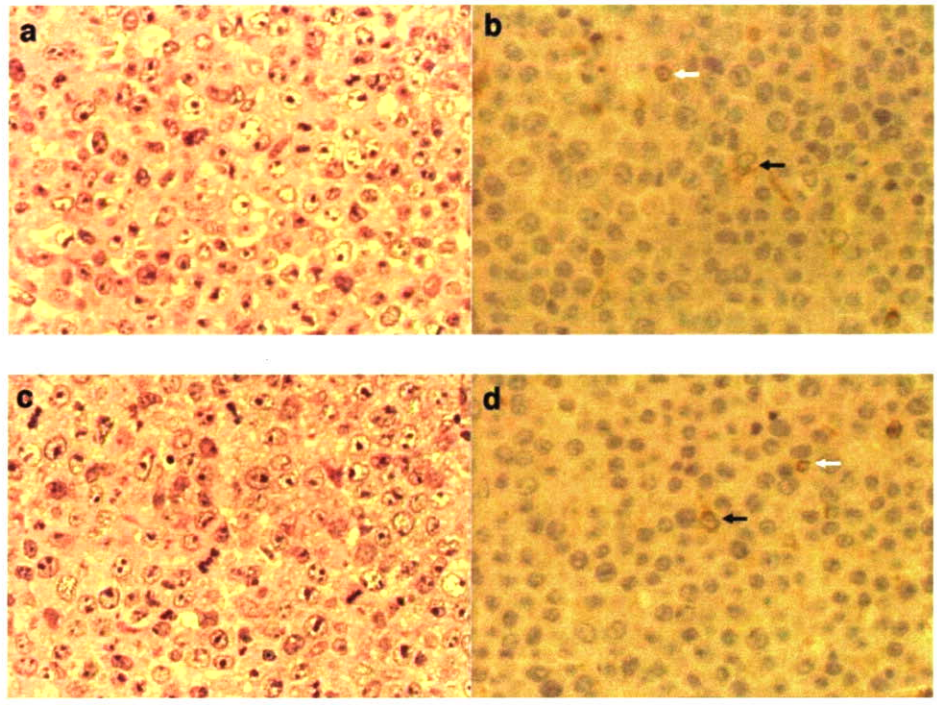

Fig. 3 Microscopic images (× 400) of HE-staining (**a**, **c**) and immunostaining with MRC OX-6 mAb for Ia antigen (**b**, **d**) in the control (**a**, **b**) and pretreated (**c**, **d**) rats bearing KDH-8 tumors. No pathological changes were observed in the tumor tissues between the untreated (control) and prednisolone-treated groups. *Black arrow* indicates macrophage infiltration; *white arrow*, lymphocyte infiltration

Uptake of FDG

FDG uptakes in the granuloma and tumor are summarized in Table 1 and Fig. 4. In the control groups, the level of FDG uptake in the granuloma was 0.909±0.142 (%ID/g) x kg which was comparable to that in the hepatoma (0.929× 0.164 (%ID/g) x kg). There was no significant difference in the level of FDG uptake between the granuloma and the tumor tissues (P=NS).

Prednisolone pretreatment significantly decreased the level of FDG uptake in the granuloma to 52% of the control value (P<0.001), while that in the tumor did not decrease significantly (85% of the control value; P=NS). The uptake levels of FDG in the granuloma and tumor tissues in the prednisolone pretreated group were 0.477± 0.139 and 0.788±0.080 (%ID/g) x kg, respectively, and the difference was significant (P<0.01) (Fig. 4).

The granuloma-to-muscle (L/M) and the granuloma-to-blood (L/B) ratios of FDG uptake were 33.5±9.7 and 9.4± 1.9 in the control group, respectively. Both the L/M ratio and L/B ratio of FDG uptake of the granuloma in the prednisolone pretreated group were significantly lower (14.4±4.0, P<0.01 for L/M ratio and 6.0±1.8, P<0.05 for L/B ratio) than those in the control group. Both the L/M ratio and L/B ratio of FDG uptake of the tumor were not significantly affected by the prednisolone pretreatment (Table 1).

Table 1 FDG uptake in granuloma and tumor

FDG uptake ((%ID/g) × kg)	Granuloma		Tumor	
	Control (n=5)	Steroid (n=6)	Control (n=6)	Steroid (n=5)
Granuloma or tumor	0.909±0.142	0.477±0.139**	0.929±0.164	0.788±0.080
Muscle	0.028±0.005	0.033±0.003	0.025±0.011	0.027±0.006
Blood	0.098±0.006	0.080±0.007**	0.060±0.017	0.054±0.015
L/M ratio	33.5±9.7	14.4±4.0**	41.0±10.9	29.6±6.0
L/B ratio	9.4±1.9	6.0±1.8*	15.9±2.4	15.3±3.2

L/M ratio, lesion (granuloma or tumor)-to-muscle ratio of FDG uptake
L/B ratio, lesion (granuloma or tumor)-to-blood ratio of FDG uptake
Control, control group; Steroid, prednisolone (PRE)-pretreated group
Data are mean±SD
*P<0.05, **P<0.01 compared with control group

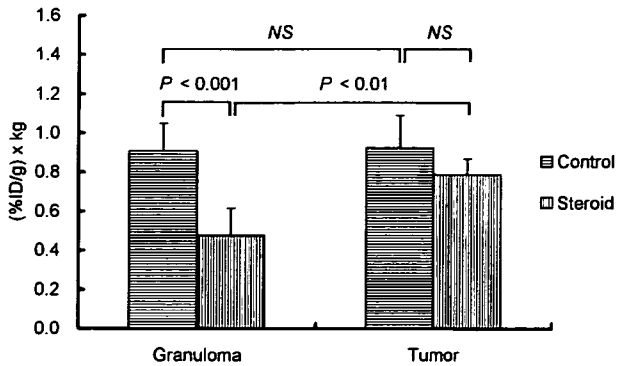

Fig. 4 FDG uptake in granuloma and tumor tissues in control and prednisolone pretreated groups. *Control* indicates the control group; *steroid* prednisolone (PRE)-pretreated group. *NS* is not statistically significant. Values given are mean ± SD

Blood glucose level and lesion weight

The blood glucose levels showed consistent tendency to increase by prednisolone pretreatment with a significant difference between the control and the pretreated rats bearing tumors (87.3±11.1 mg/dl vs 124.8±11.7 mg/dl at the time of FDG intravenous injection, $P<0.05$) (Table 2). The granuloma weight was significantly reduced by the prednisolone pretreatment (0.137±0.027 g for control rats and 0.089±0.024 g for pretreated rats, $P<0.05$), while the tumor weight was not (4.435±1.806 g for control rats and 4.085±2.083 g for pretreated rats, P=NS). There were no significant differences in the body weight of rats among all groups (Table 2).

PET images

Figure 5 shows representative FDG-PET images of rats bearing BCG granulomas or KDH-8 tumors before and after a prednisolone treatment. BCG granulomas and tumors were clearly visualized before the prednisolone treatment (Fig. 5a and c, control). Prednisolone treatment markedly reduced the uptake of FDG in BCG granulomas (Fig. 5b), but not in tumors (Fig. 5d).

Discussion

In this study, we developed an intramuscular granuloma rat model characterized by epithelioid cell granuloma-formation and massive lymphocyte-infiltration around the granuloma (Fig. 1a and b), histologically similar to those observed in sarcoidosis [11]. The granuloma showed high FDG uptake comparable to that of the tumor (Figs. 4 and 5). In addition, the present study demonstrated that the effect of prednisolone pretreatment on FDG uptake was greater in the granulomatous lesions than that in the tumor (Figs. 4 and 5). These results suggest that BCG-induced granuloma may be a valuable model and may provide a biological basis for FDG studies.

In our model, extensive FDG uptake was observed in the granuloma, which was comparable to that in the tumor. To the best of our knowledge, there have been no studies showing a comparison of FDG uptake in experimental granulomas and tumors, although increased FDG uptake in inflammatory lesions has been reported in experimental inflammation induced by an intramuscular injection of *S. aureus* or turpentine oil [5, 6]. In our previous study, the inflammatory lesions induced by *S. aureus* and turpentine oil showed levels of FDG uptake which were about 45% and 34% of that in KDH-8 tumor, respectively [6]. van Waarde et al. also suggested that FDG uptake in the turpentine oil-induced inflammatory lesion was about 35% of that in C6 rat glioma [5]. *S. aureus* and turpentine-induced inflammatory tissues showed massive neutrophil-infiltration and ambient connective tissue-formation around the injection sites of *S. aureus* and turpentine oil. Increased FDG distribution was mainly shown in the areas of neutrophil-infiltration, and FDG distribution was lower in the ambient connective tissues. On the contrary, in our granuloma model, increased FDG distribution was mainly shown in the epithelioid cell granulomas by our preliminary experiments using autoradiography (data not shown). The activities of granuloma formation and granuloma-associated immune cells may be reflected by FDG accumulation, although detailed mechanisms of the accumulation occur-

Table 2 Blood glucose level and body and lesions weights

		Granuloma		Tumor	
	Parameter	Control (n=5)	Steroid (n=6)	Control (n=6)	Steroid (n=5)
Blood glucose (mg/dl)	0 min	87.0±9.3	95.7±8.3	87.3±11.1	124.8±11.7*
	60 min	79.6±6.6	87.0±10.0	86.7±8.8	96.8±11.4
	Body weight (kg)	0.270±0.015	0.260±0.013	0.235±0.030	0.239±0.029
	Lesion weight (g)	0.137±0.027	0.089±0.024*	4.435±1.806	4.085±2.083

0 min at FDG injection; 60 min at sacrifice; Control indicates the control group; steroid, the prednisolone (PRE)-pretreated group
Data are mean ± SD
*$P<0.05$ compared with control group

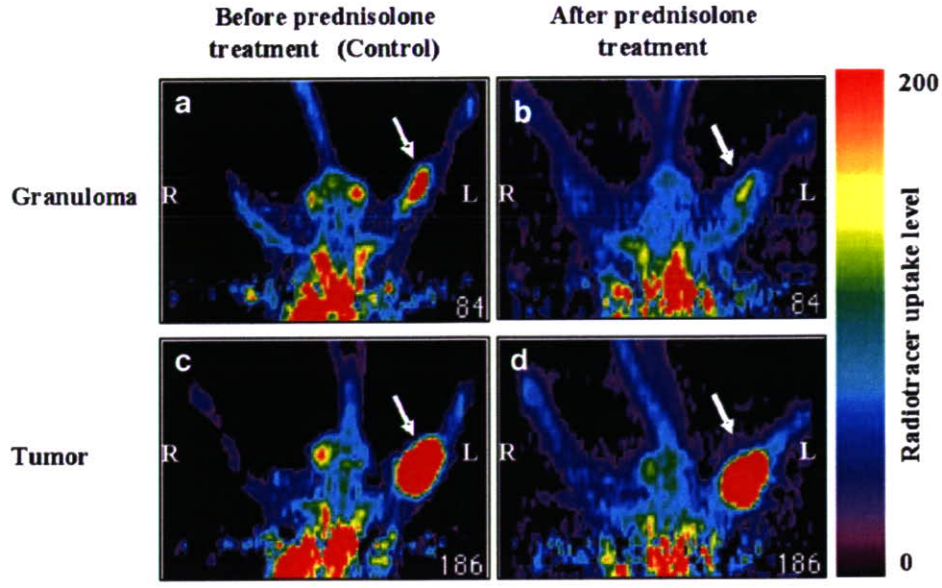

Fig. 5 FDG-PET images of rats bearing BCG granulomas (**a** and **b**) or KDH-8 tumors (**c** and **d**). Horizontal PET images before (**a** and **c**) and after prednisolone treatment (**b** and **d**) are shown. *Arrows* indicate the locations of BCG granulomas (**a** and **b**) and KDH-8 tumors (**c** and **d**) inoculated in the left calf muscles of rats. Color scale depicts radiotracer uptake level normalized to animal body weight and injected dose. *R* indicates right; *L*, left

ring in the granuloma remain unclarified. The animal models of inflammation induced by *S. aureus* and turpentine oil may not be suitable models for differentiating malignant tumors from benign diseases because of the relatively low FDG uptake levels in their inflammatory lesions. In contrast, our granuloma rat model showed a high FDG uptake in the granulomatous lesions comparable to that in the KDH-8 tumor, indicating the suitability of our model for such studies.

Our intramuscular granuloma rat model showed histologically similar characteristics to sarcoidosis [11, 12], as shown in Figs. 1 and 2. Sarcoidosis is a main source of false-positive FDG-PET findings in oncology. Sarcoidosis can be characterized in the affected organs by an accumulation of activated macrophages (epithelioid cells and multinuclear giant cells) and activated T lymphocytes at the site of disease activity. Pathologically, the first manifestation of the disease is an accumulation of mononuclear inflammatory cells, mainly CD4+ T helper 1 lymphocytes and mononuclear phagocytes in the affected organ. This inflammatory process is followed by the formation of granulomas, and aggregations of macrophages and their progeny, epithelioid cells, and multinucleated giant cells [13, 14]. This study showed the accumulation of epithelioid cells and macrophages defined by positive staining with RM-4 (Fig. 2c) in the granuloma, and CD4+ lymphocytes into the periphery of the granuloma (Fig. 2d), indicating the histological similarity of our model to sarcoidosis [9]. The cellular uptake of FDG in sarcoidosis is considered to be related to its inflammatory cell infiltrates, which are composed of lymphocytes, macrophages, and epithelioid cells from monocytes, because FDG has been observed in vitro to be accumulated by leukocytes [15, 16], lymphocytes, and macrophages [17]. The histological similarity of our granuloma rat model to sarcoidosis indicates its potential for providing a biological basis for differentiating sarcoidosis from malignant tumors, although detailed investigations, including those on FDG distribution at the cellular level, are required.

The immune-associated (Ia) antigen represents a 23,000- and 30,000-dalton membrane glycoprotein complex. The Ia antigen is normally expressed on all B-lymphocytes and some monocytes, but not in large amounts on normal T cells unless they are activated by allogenic or mitogenic stimulation [18]. The expression of Ia antigen on T cells is a sign of T cell activation in active sarcoidosis [19]. The present study also showed the accumulation of Ia positive (Ia^+) epithelioid cells and macrophages in the granuloma and Ia^+ lymphocytes into the periphery of the granuloma (Figs. 1, 2a and b), which further support the histological similarity of our model to sarcoidosis [9]. The extensive FDG uptake in the granuloma was decreased by prednisolone pretreatment, being concordant with the reduction in epithelioid cell granuloma-formation and lymphocyte-infiltration, including the infiltrations of Ia^+ macrophages and Ia^+ lymphocytes (Figs. 1c and d, 4b). These results suggest that FDG uptake might reflect active granulomatous processes.

For almost four decades, oral corticosteroids have been the mainstay of treatment in pulmonary sarcoidosis [20, 21]. To elucidate the mechanism of glucocorticoid on the suppressive course of the reaction to granulomatous lung tissue in experimental pulmonary granulomas, Gemma et al. [8] have performed immunohistochemical staining of an Ia+ antigen at 1 and 2 days after high-dose prednisolone treatment. The results showed a remarkable reduction in the number of Ia+ macrophages and Ia+ lymphocytes in the granulomatous lung tissue after the treatment with predni-

olone. These findings suggest that glucocorticoid may suppress the immunological activities of macrophages and T cells through their inhibitory effect on the differentiation of Ia+ macrophages and activated T cells, which may result in the diminishment of the pulmonary granulomatous reaction through the disorder of the macrophage-T cell interaction. In patients with pulmonary sarcoidosis, FDG uptake in the lung was decreased after high-dose steroid therapy concordant with the histologic activity in the lung [2, 3, 14]. The present study showed that prednisolone pretreatment significantly decreased the level of FDG uptake in the granuloma to 52% of the control value (Table 1, Fig. 4). Our histological findings showed that the Ia^+ macrophage-infiltration, epithelioid cell granuloma-formation, and activated T lymphocyte-infiltration in the granuloma were decreased by prednisolone pretreatment. The decreased FDG uptake in the granuloma by the steroid pretreatment may be ascribed to the reduced histologic activity, including epithelioid cell granuloma-formation and lymphocyte-infiltration. The current results are in accordance with those in patients with pulmonary sarcoidosis [2, 3, 19]. On the other hand, the level of FDG uptake and histological features of the tumor were not significantly affected by the prednisolone pretreatment. Taken together, corticosteroid pretreatment may provide a potential means for differentiating malignant tumors from granulomatous lesions in FDG-PET studies, although further studies in other animal models and in patients are needed to confirm the present results.

In this study, to generate experimental tumors, allogenic hepatoma cells (KDH-8) were inoculated into the left calf muscle of rats. The histopathological characterization of intramuscular tumor tissues showed massive viable and proliferating cancer cells by HE staining and few Ia+ macrophage-infiltration and Ia+ lymphocyte-infiltration defined by the MRC OX-6 mAb into viable tumor cells 14 days after the inoculation of KDH-8. However, the inflammatory cells could seldom be seen around the tumor graft by HE and immunohistochemical stains. Hashimoto et al. [22] have also reported that the lesion consisted of many viable tumor cells with few tumor-tissue infiltrating lymphocytes in the tumor and several granulocytes and macrophages at the center of the tumor bearing into the leg muscle of WKAH rats 14 days after inoculation of KDH-8. In the present study, FDG uptake level in the tumor was decreased slightly after prednisolone treatment, although the difference was not significant (85% of the control value). On the other hand, there were no obvious histopathological changes in the tumor tissue after prednisolone treatment (Fig. 3c and d). Accordingly, the anti-inflammatory/immune effects of prednisolone may not be responsible for the reduction in tumoral FDG uptake level. Elevated blood glucose levels induced by corticosteroid and the antitumoral effects of prednisolone may be other explanations for the reduction in the tumoral FDG uptake level.

In the present study, the blood glucose levels showed consistent tendency to increase by the prednisolone pretreatment with a significant difference between the control and pretreated rats bearing tumor. It is well known that the action of steroids on glucose metabolism increases the blood glucose level [23, 24]. The uptake of FDG in tissues is affected by the blood glucose level [25, 26]. Accordingly, the reduced FDG uptake in the granuloma and tumor may be partly ascribed to the elevated blood glucose levels. However, the effect of prednisolone pretreatment on FDG uptake was greater in the granuloma than in the tumor, although the elevation in the blood glucose level was higher in rats bearing tumor. A slight elevation in the blood glucose level (125 mg/dl) following PRE pretreatment may not affect the uptake levels of FDG in the tumor, as reported previously [5, 27]. Detailed investigations, including quantitative evaluation of inflammation levels (i.e., determination of inflammatory cell density) and autoradiographic studies using FDG, are required to clarify the reason for the reduction in tumoral FDG uptake level.

As mentioned above, it is of great importance to clarify the detailed FDG distribution at the cellular level in the granuloma. In this regard, Kubota et al. reported a high FDG accumulation in young granulation tissues around the tumor and in the macrophages infiltrating the marginal areas surrounding the extensive tumor necrosis by micro-autoradiographies of FDG and ^{3}H-DG [17]. Activated inflammatory cells have markedly increased glycolysis. The hexose monophosphate shunt is stimulated by phagocytosis, which is enhanced 20–30-fold that of baseline values which is the cause of the high FDG uptake [28]. Although microautoradiographic studies of ^{3}H-FDG or ^{14}C-FDG are needed to clarify the detailed FDG distribution at the cellular level in our granuloma rat model, the results of this study indicate that a high FDG uptake in the granuloma is related to the activation of inflammatory cell infiltrates, including mature epithelioid cells, massive macrophages, and lymphocytes.

The PET images showed that BCG granuloma and tumors were clearly visualized before the prednisolone treatment (Fig. 5a and c, control). Prednisolone treatment markedly reduced FDG uptake in BCG granulomas but not in tumors (Fig. 5b and d). These results demonstrate that PET is a useful noninvasive imaging method to depict and assess early changes in FDG uptake by the corticosteroid treatment.

Low-grade hepatocellular carcinoma (HCC) has a low FDG uptake level due to its histological characteristics of being closer to the normal liver, which has abundant glucose-6-phophatase. However, high-grade HCC, intra-

and extrahepatic metastases, and distant metastases correlated with positivity of FDG-PET. Thus, FDG-PET imaging has a clinically significant impact on the management of patients diagnosed with HCC [29]. KDH-8 is a rat transplantable hepatocellular carcinoma that is found in WKAH rats and is histologically poorly undifferentiated. Our previous study showed that the FDG uptake level in the hepatoma was the same as or higher than that in the other tumor models [5]. Our hepatoma model, employed as an extrahepatic metastase, should provide a biological basis for evaluating the impact of FDG imaging on the management of patients diagnosed with hepatocellular carcinoma.

It should be noted that there are several limitations to our study. First, each rat was inoculated with BCG granulomas or KDH-8 tumors in this study because FDG uptake may be affected if both the BCG granulomas and the KDH-8 tumors were inoculated into the same rat. However, it is possible to inject BCG and KDH-8 cells in the same animal, and a rat model bearing both the BCG granulomas and the KDH-8 tumors may be useful to determine the differences in FDG uptake profiles between the granulomas and tumors. Second, anesthesia may affect FDG uptake, as the rats were kept under pentobarbital anesthesia during FDG uptake. In this regard, Lee et al. have reported that pentobarbital injection elevated blood FDG activity to 2.0-fold higher than the control levels, but had no effect on tumor uptake [30]. Recently, we compared the effects of pentobarbital and ketamine/medetomidine on FDG uptake in a rat model bearing KDH-8 tumors. The results showed no change in FDG uptake levels for either anesthetic agent. The effects of anesthesia on FDG uptake in tumors appeared to be small, compared with those in the brain. Finally, it is important to quantify the level of inflammation for FDG uptake correlation studies. Unfortunately, we could not perform quantitative evaluation of inflammation levels, which prevented us to accurately evaluate the correlation between the level of inflammation and FDG uptake level in the tumors and granulomas. Although our findings show that the pathological characterization of the BCG granulomas was similar to that of sarcoidosis, and FDG accumulation level was decreased by steroid treatment, detailed investigations, including quantitative evaluation of inflammation levels (i.e., determination of inflammatory cell density) and autoradiographic studies using FDG, are required to accurately evaluate the correlation between the level of inflammation and FDG distribution.

Conclusion

In the present study, we developed a BCG-induced granuloma rat model which has similar histopathological features as those of sarcoidosis. The granuloma showed a high FDG uptake comparable to that of the tumor. In addition, our results demonstrate that the effect of prednisolone pretreatment on FDG uptake was greater in the granuloma than in the tumor. These results suggest the usefulness of our model for studying FDG accumulation in inflammatory lesions.

Acknowledgments This work was supported in part by a grant-in-aid for Scientific Research from the Japan Society for the Promotion of Science, by a grant-in-aid for Scientific Research from the Japanese Ministry of Education, Culture, Sports, Science and Technology, by Special Coordination Funds for Promoting Science and Technology provided by the Ministry of Education, Culture, Sports, Science and Technology, the Japanese Government, by a Grant-in-Aid for Cancer Research from the Ministry of Health and Welfare of Japan, and by a grant from the Rotary Yoneyama Memorial Foundation, Inc. The authors are grateful to the staff members of the Department of Nuclear Medicine, Central Institute of Isotope Science and Institute for Animal Experimentation, Hokkaido University and the Facility of Radiology, Hokkaido University Hospital, for supporting this study. We also thank Eriko Suzuki, secretary of the professor of the Department of Nuclear Medicine, Hokkaido University, for continuously supporting this study and Makoto Sato, SHI Accelerator Service Ltd., for FDG syntheses.

References

1. Dimitrakopoulou-Strauss A, Strauss LG, Heichel T, Wu H, Burger C, Bernd L, et al. The role of quantitative (18)F-FDG PET studies for the differentiation of malignant and benign bone lesions. J Nucl Med 2002;43:510–8.
2. Brudin LH, Valind S, Rhodes CG, Pantin CF, Sweatman M, Jones T, et al. Fluorine-18 deoxyglucose uptake in sarcoidosis measured with positron emission tomography. Eur J Nucl Med 1994;21:297–305.
3. Lewis PJ, Salama A. Uptake of fluorine-18-fluorodeoxyglucose in sarcoidosis. J Nucl Med 1994;35:1647–9.
4. Ohtsuka T, Nomori H, Watanabe K, Naruke T, Orikasa H, Yamazaki K, et al. False-positive findings on [18F]FDG-PET caused by non-neoplastic cellular elements after neoadjuvant chemoradiotherapy for non-small cell lung cancer. Jpn J Clin Oncol 2005;35:271–3.
5. van Waarde A, Cobben DC, Suurmeijer AJ, Maas B, Vaalburg W, de Vries EF, et al. Selectivity of 18F-FLT and FDG for differentiating tumor from inflammation in a rodent model. J Nucl Med 2004;45:695–700.
6. Zhao S, Kuge Y, Tsukamoto E, Mochizuki T, Kato T, Hikosaka K, et al. Effects of insulin and glucose loading on FDG uptake in experimental malignant tumours and inflammatory lesions. Eur J Nucl Med 2001;28:730–5.
7. Zhao S, Kuge Y, Mochizuki T, Takahashi T, Nakada K, Sato M, et al. Biologic correlates of intratumoral heterogeneity in FDG distribution with regional expression of glucose transporters and hexokinase-II in experimental tumor. J Nucl Med 2005;46:675–82.
8. Gemma H, Sato A. Effect of glucocorticoid on lung tissue and bronchus-associated lymphoid tissue of experimental granulomatous lung. Kekkaku 1989;64:387–99.
9. Whiteland JL, Nicholls SM, Shimeld C, Easty DL, Williams NA, Hill TJ. Immunohistochemical detection of T-cell subsets

and other leukocytes in paraffin-embedded rat and mouse tissues with monoclonal antibodies. J Histochem Cytochem 1995;43: 313–20.
10. Watanabe M, Okada H, Shimizu K, Omura T, Yoshikawa E, Kosugi T, et al. A high resolution animal PET scanner using compact PS-PMT detectors. IEEE Trans Nucl Sci 1997;44:1277–82.
11. Schrier DJ, Ripani LM, Katzenstein AL, Moore VL. Role of angiotensin-converting enzyme in bacille Calmette-Guerin-induced granulomatous inflammation. Increased angiotensin-converting enzyme levels in lung lavage and suppression of inflammation with captopril. J Clin Invest 1982;69:651–7.
12. Sandor M, Weinstock JV, Wynn TA. Granulomas in schistosome and mycobacterial infections: a model of local immune responses. Trends Immunol 2003;24:44–52.
13. Chang JM, Lee HJ, Goo JM, Lee HY, Lee JJ, Chung JK, et al. False positive and false negative FDG-PET scans in various thoracic diseases. Korean J Radiol 2006;7:57–69.
14. du Bois RM. Corticosteroids in sarcoidosis: friend or foe? Eur Respir J 1994;7:1203–9.
15. Osman S, Danpure HJ. The use of 2-[18F]fluoro-2-deoxy-D-glucose as a potential in vitro agent for labeling human granulocytes for clinical studies by positron emission tomography. Int J Rad Appl Instrum B 1992;19:183–90.
16. Borregaard N, Herlin T. Energy metabolism of human neutrophils during phagocytosis. J Clin Invest 1982;70:550–7.
17. Kubota R, Yamada S, Kubota K, Ishiwata K, Tamahashi N, Ido T. Intratumoral distribution of fluorine-18-fluorodeoxyglucose in vivo: high accumulation in macrophages and granulation tissues studied by microautoradiography. J Nucl Med 1992;33:1972–80.
18. Winchester RJ, Kunkel HG. The human Ia system. Adv Immunol 1979;28:221–92.
19. Costabel U, Bross KJ, Ruhle KH, Lohr GW, Matthys H. Ia-like antigens on T-cells and their subpopulations in pulmonary sarcoidosis and in hypersensitivity pneumonitis. Analysis of bronchoalveolar and blood lymphocytes. Am Rev Respir Dis 1985;131:337–42.
20. Siltzbach LE. Effects of cortisone in sarcoidosis: a study of thirteen patients. Am J Med 1952;12:139–60.
21. Milman N. Oral and inhaled corticosteroids in the treatment of pulmonary sarcoidosis—a critical reappraisal. Sarcoidosis Vasc Diffuse Lung Dis 1998;15:150–7.
22. Hashimoto S, Shirato H, Hosokawa M, Nishioka T, Kuramitsu Y, Matushita K, et al. The suppression of metastases and the change in host immune response after low-dose total-body irradiation in tumor-bearing rats. Radiat Res 1999;151:717–24.
23. West KM. Comparison of the hyperglycemic effects of glucocorticoids in human beings; the effect of heredity on responses to glucocorticoids. Diabetes 1957;6:168–75.
24. Pellacani A, Fornengo P, Bruno A, Ceruti C, Mioletti S, Curto M, et al. Acute methylprednisolone administration induces a transient alteration of glucose tolerance and pyruvate dehydrogenase in humans. Eur J Clin Invest 1999;29:861–7.
25. Wahl RL, Henry CA, Ethier SP. Serum glucose: effects on tumor and normal tissue accumulation of 2-[F-18]-fluoro-2-deoxy-D-glucose in rodents with mammary carcinoma. Radiology 1992;183:643–7.
26. Lindholm P, Minn H, Leskinen-Kallio S, Bergman J, Ruotsalainen U, Joensuu H. Influence of the blood glucose concentration on FDG uptake in cancer—a PET study. J Nucl Med 1993;34:1–6.
27. Zhao S, Kuge Y, Nakada K, Mochizuki T, Takei T, Okada F, et al. Effect of steroids on [18F]fluorodeoxyglucose uptake in an experimental tumour model. Nucl Med Commun 2004;25:727–30.
28. Amrein PC, Larson SM, Wagner HN Jr. An automated system for measurement of leukocyte metabolism. J Nucl Med 1974; 15:352–5.
29. Wudel LJ Jr, Delbeke D, Morris D, Rice M, Washington MK, Shyr Y, et al. The role of [18F]fluorodeoxyglucose positron emission tomography imaging in the evaluation of hepatocellular carcinoma. Am Surg 2003; 69:117–24.
30. Lee KH, Ko BH, Paik JY, Jung KH, Choe YS, Choi Y, et. al. Effects of anesthetic agents and fasting duration on 18F-FDG biodistribution and insulin levels in tumor-bearing mice. J Nucl Med 2005;46:1531–6.

Ann Nucl Med (2007) 21:331–337
DOI 10.1007/s12149-007-0035-x

ORIGINAL ARTICLE

Comparison of MET-PET and FDG-PET for differentiation between benign lesions and lung cancer in pneumoconiosis

**Kakuko Kanegae · Ikuo Nakano · Kiyonobu Kimura
Hiroshi Kaji · Yuji Kuge · Tohru Shiga · Songji Zhao
Shouzo Okamoto · Nagara Tamaki**

Received: 5 December 2006 / Accepted: 10 April 2007

Abstract
Objective The aim of this study was to evaluate and compare the ability of C-11-methionine (MET) and F-18 fluoro-deoxy-D-glucose positron emission tomography (FDG-PET) to diagnose lung cancer in patients with pneumoconiosis.
Methods Twenty-six subjects underwent both whole-body MET-PET and FDG-PET on the same day. The first group was a lung cancer group, which consisted of 15 patients, and included those with pneumoconiosis with increased nodules (13 cases), hemoptysis (1 case), and positive sputum cytology (1 case). The second group was a no-malignancy control group, consisting of 11 patients with pneumoconiosis.
Results Significant correlations between nodule size and the maximum standardized uptake value (SUV_{max}) of the two PET tracers were observed in the control group. The larger the nodule size, the greater were the amounts of these tracers accumulated (MET: $r = 0.771$, $P < 0.0001$; FDG: $r = 0.903$, $P < 0.0001$). The SUV_{max} of MET was significantly lower than that of FDG in the pneumoconiotic nodules ($P < 0.0001$). Lung cancer was found in 5 of 19 nodules (two with adenocarcinoma, one with squamous cell carcinoma, one with small cell carcinoma, and one with large cell carcinoma) in the first group. As for nodules equal to or less than 3 cm in diameter, the SUV_{max} of MET was significantly higher in the lung cancer than in the pneumoconiotic nodules, with 3.48 ± 1.18 (mean ± SE) for the lung cancer and 1.48 ± 0.08 for the pneumoconiotic nodules ($P < 0.01$), similar to the SUV_{max} of FDG, with 7.12 ± 2.36 and 2.85 ± 0.24 ($P < 0.05$), respectively. On the basis of the criteria for the control group, FDG and MET identified lung cancer with sensitivities of 60% and 80%, specificities of 100% and 93%, accuracies of 90% and 90%, positive predictive values of 100% and 80%, and negative predictive values of 88% and 93%, respectively.
Conclusions Our results indicate that nodules with an intense uptake of MET and FDG relative to their size should be carefully observed because of a high risk for lung cancer.

Keywords FDG · PET · C-11-methionine · Pneumoconiosis · Lung cancer

K. Kanegae (✉) · T. Shiga · S. Zhao · S. Okamoto · N. Tamaki
Department of Nuclear Medicine, Hokkaido University Graduate School of Medicine, Kita 15, Nishi 7, Kita-ku, Sapporo 060-8638, Japan
e-mail: IZW00143@nifty.com

I. Nakano · K. Kimura · H. Kaji
Iwamizawa Rousai Hospital, Iwamizawa, Japan

Y. Kuge
Department of Molecular Imaging, Hokkaido University Graduate School of Medicine, Sapporo, Japan

Introduction

Patients with pneumoconiosis are at high risk for developing lung cancer, but it is difficult to differentiate lung cancer from benign pneumoconiosis on conventional imaging such as X-ray and computed tomography (CT). 2-[^{18}F]-fluoro-deoxy-D-glucose (FDG) and L-methyl-[^{11}C]-methionine (MET) are commonly used as tumor-seeking positron emission tomography (PET) tracers. However, in patients with pneumoconiosis, either of these tracers may show a false-positive finding in differentiating lung cancer from benign lesions, because of the avid uptake of these tracers in benign lesions such as

inflammatory/granulomatous lesions and pneumoconiotic nodules [1–7]. We hypothesized that the degrees of accumulations of the two PET tracers in pneumoconiotic nodules would be size dependent. Quantitative assessment of uptake of these tracers relative to the size of the lesions may improve the diagnostic accuracy for differentiating malignant and benign lesions in these patients. This report describes the first clinical study for the quantitative assessment of MET uptake on PET in pneumoconiosis and lung cancer, and compares the findings with those of FDG-PET.

The purpose of this study was to quantitatively assess and compare the values of both MET-PET and FDG-PET for prospectively differentiating between benign lesions and lung cancers in pneumoconiotic lungs.

Materials and methods

Subjects

A total of 26 patients with pneumoconiosis were prospectively examined at Hokkaido University Hospital, Sapporo, Japan, from September 2005 to October 2006. All patients were selected from clinical patients at the Iwamizawa Rousai Hospital who were referred for an evaluation of pneumoconiosis. Of the 26 patients, 24 were former coal miners, 1 was a former metal miner, and 1 was a coal analysis employee.

Two groups were created according to the patient's diagnosed status before two PET examinations. The first was a suspected lung cancer group, which consisted of 15 patients with pneumoconiosis (15 men, age range 61–82 years, mean age 71 ± 6 years), and included those with increased nodules (13 cases), hemoptysis (1 case), and positive sputum cytology (1 case). These patients had a mean body weight of 57.9 ± 7.6 kg and a mean fasting glucose level of 93.9 ± 14.3 mg/dl. The second group was a no-malignancy control group, consisting of 11 patients with pneumoconiosis (11 men, age range 63–76 years, mean age 72 ± 5 years) having a mean body weight of 61.9 ± 6.0 kg and a mean fasting glucose level of 93.0 ± 9.9 mg/dl. These subjects had no evidence of lung cancer, which was confirmed on the basis of a long-term follow-up to date.

PET protocol

The 26 subjects underwent both whole-body MET-PET and FDG-PET on the same day. Written informed consent was obtained from all the patients before performing the PET studies. A whole-body MET-PET image was obtained from 15 min to 20 min after the injection of 491.0 ± 60.7 MBq (mean ± SD, range 361–607 MBq) of MET. One hour later, 237.7 ± 49.4 MBq (mean ± SD, range 161–339 MBq) of FDG was administered to obtain a whole-body FDG-PET image from 40 min to 60 min after injection. The day before the PET studies, the patients in both groups were requested to fast for at least 6 h before the scheduled FDG injection. Whole-body PET acquisitions were carried out from the skull base to the pelvis with a 2-min emission scan and a 3-min transmission scan per bed, using a PET scanner (Siemens EXACT 47) in the 3D mode. Non-attenuation correction images were reconstructed with the filtered back projection method. Attenuation correction was performed using rotating ^{68}Ge–^{68}Ga rod sources. The scans were reconstructed with the ordered subsets expectation maximization algorithm.

Data analysis

Both the MET and FDG uptakes were evaluated using the maximum standardized uptake value (SUV_{max}), as reported earlier [8, 9]. Nodule size was determined using the maximal diameter of the nodule on CT. The differences in SUV_{max} between FDG and MET in the control group, and the differences between pneumoconiotic nodules and lung cancer for nodules measuring 3 cm or less where the tracer had accumulated, were examined using the nonparametric test (Mann–Whitney U test). $P < 0.05$ was considered to be statistically significant.

Results

The correlations between pneumoconiotic nodule size and the degrees of FDG and MET accumulations for 39 nodules in the control group were examined. A significant correlation between nodule size and the SUV_{max} of the two PET tracers was observed in pneumoconiosis. The larger the nodule size, the greater were the amounts of these tracers accumulated (MET: $r = 0.771$, FDG: $r = 0.903$; Figs. 1, 2). The SUV_{max} of MET was significantly lower than that of FDG in pneumoconiotic nodules ($P < 0.0001$).

There were 19 nodules suspected of being malignant in the 15 patients in the first group. Table 1 shows a summary of the final diagnosis of the lung lesions in these 15 patients. Lung cancer was detected in 5 of the 19 nodules (two with adenocarcinoma, one with squamous cell carcinoma, one with small cell carcinoma, and one with large cell carcinoma). The final diagnosis was histologically determined in three patients and cytologically determined in two patients. The remaining 10 patients had 14 benign lesions, of which 3 were inflam-

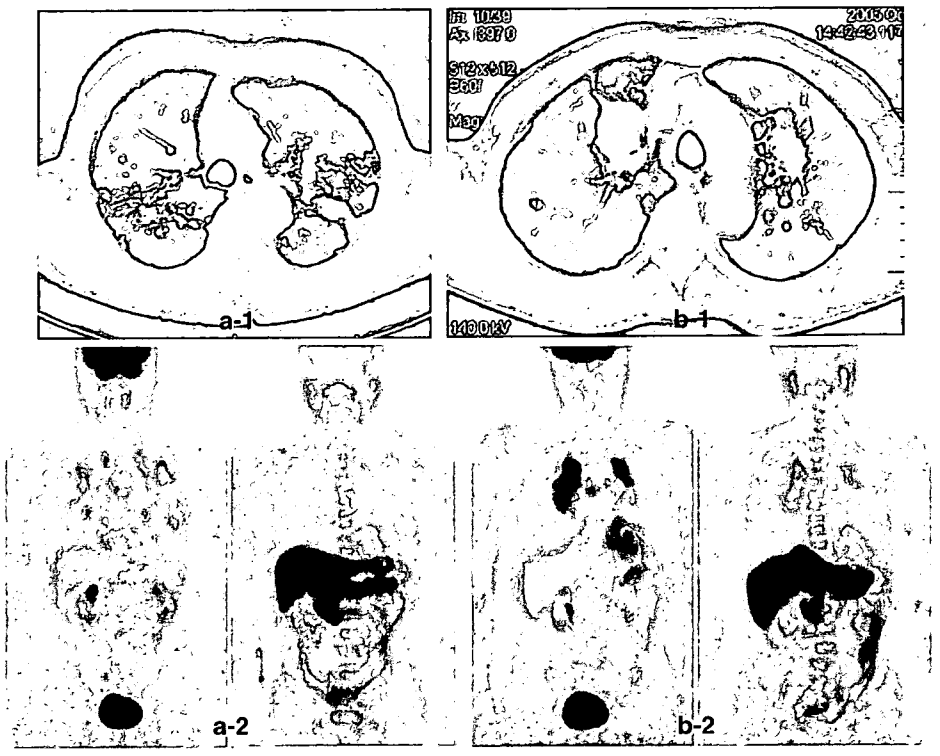

Fig. 1 Computed tomography (CT) images of small multiple pneumoconiotic nodules (**a-1**) and large pneumoconiotic nodules (**b-1**) in the control group. The degree of the accumulation of 11-C-methionine (MET: **a-2**, **b-2**; *right*) was size dependent as well as that of fluoro-deoxy-D-glucose (FDG: **a-2**, **b-2**; *left*)

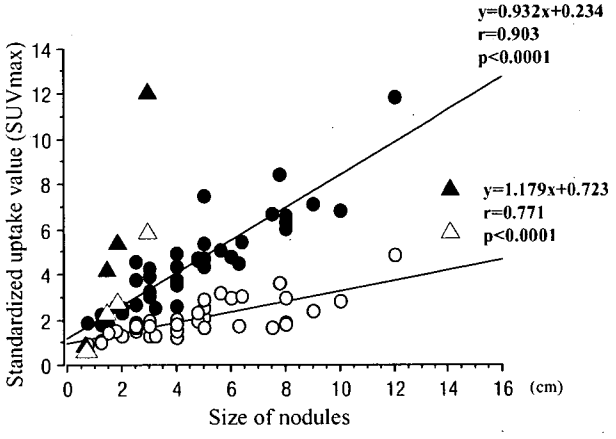

Fig. 2 Correlation between the nodule size of pneumoconiosis and regional tracer uptake (maximum standardized uptake value, SUV_{max}) in control group. Significant correlations between the nodular size and SUV_{max} of the two positron emission tomography (PET) tracers were observed in pneumoconiosis. The SUV_{max} of MET was significantly lower than that of FDG in pneumoconiotic nodules. *Open circle*, MET (pneumoconiotic nodule); *filled circle*, FDG (pneumoconiotic nodule); *open triangle*, MET (lung cancer); *filled triangle*, FDG (lung cancer)

matory lesions and 11 pneumoconiotic nodules. The diagnosis was histologically determined in one patient, bacteriologically determined in one patient, and clinically determined on the basis of the clinical course in eight patients.

Table 1 Diagnosis of 19 nodules in suspected lung cancer group

Lung cancer	5
Adenocarcinoma	2
Squamous cell carcinoma	1
Small cell carcinoma	1
Large cell carcinoma	1
Benign lesion	14
Infection/inflammation	3
Pneumoconiotic nodule	11

When three lung cancers were compared with the pneumoconiotic nodules measuring 3 cm or less in diameter of the control group and in which the tracer had accumulated, a significant difference was observed in the accumulation in both cases (Fig. 3). The SUV_{max} of MET was significantly higher in lung cancer than in pneumoconiotic nodules, with 3.48 ± 1.18 (mean ± SE) for the lung cancer and 1.48 ± 0.08 for the pneumoconiotic nodules ($P < 0.01$), similar to the SUV_{max} of FDG with 7.12 ± 2.36 and 2.85 ± 0.24 ($P < 0.05$), respectively. Because of the limited number of lung cancers with pneumoconiosis, the reliability of the statistical analysis was less than usual.

Table 2 shows the SUV_{max} of pneumoconiotic nodules in the control group as the criterion for differentiating malignant nodules from benign lesions. In small nodules of pneumoconiosis, 3 cm or less, the mean SUV_{max} of FDG and MET were 2.85 ± 0.93 (SD) and 1.48 ± 0.31,

respectively. In nodules more than 3cm, the mean SUV_{max} of FDG and MET were 5.56 ± 2.00 and 2.34 ± 0.84, respectively.

On the basis of these criteria from the control group, FDG and MET identified lung cancer with sensitivities of 60% (3/5) and 80% (4/5), specificities of 100% (14/14) and 93% (13/14), accuracies of 90% (17/19) and 90% (17/19), positive predictive values of 100% (3/3) and 80% (4/5), and negative predictive values of 88% (14/16) and 93% (13/14), respectively.

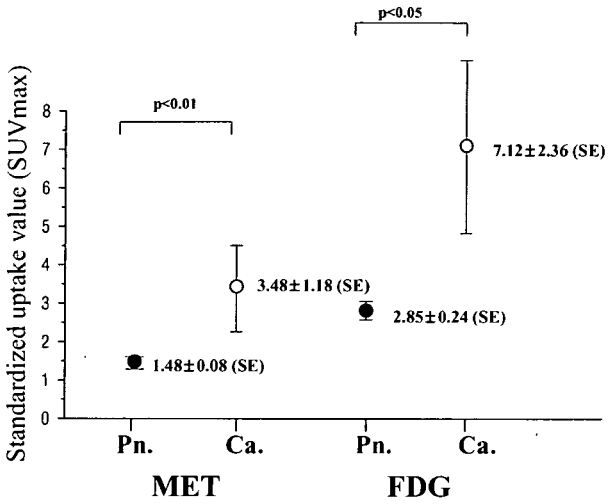

Fig. 3 Differential diagnosis of small nodules (3cm or less) using MET-PET and FDG-PET. SUV_{max} of three lung cancers was significantly higher than that of 15 pneumoconiotic nodules in control group. *Pn.*, pneumoconiotic nodule; *Ca.*, lung cancer

Table 2 Maximum standardized uptake value (SUV_{max}) of pneumoconiotic nodules in the control group

	SUV_{max} (mean ± SD)	
	FDG	MET
≤3cm	2.85 ± 0.93	1.48 ± 0.31
3cm <	5.56 ± 2.00	2.34 ± 0.84

FDG 2-[^{18}F]-fluoro-deoxy-D-glucose, *MET* C-11-methionine

Table 3 shows results of the evaluation of lung cancer in comparison with the control group. Three of 5 cases were properly diagnosed to have lung cancer by both FDG and MET-PET (Fig. 4). We were able to indicate the presence of malignancy in the case of a 2-cm-long squamous cell carcinoma of the lung hilum with FDG-PET SUV_{max} of 11.76 and MET-PET SUV_{max} of 5.81. It was difficult to evaluate one case of small (0.7cm in diameter) well-differentiated adenocarcinoma in which no accumulation was observed by either FDG or MET. In the case of a large cell carcinoma (14cm; Fig. 5), intense uptake of FDG in the large bulky nodule but focal and high MET uptake in lower portion of the large nodule suggested lung cancer. In this case, lung cancer was highly suspected with MET-PET with false-negative finding on FDG-PET. Of the remaining 14 nodules without lung cancer in the first group, 11 pneumoconiotic nodules in 7 patients showed similar FDG (SUV_{max} range 1.00–4.46, mean 3.04) and MET (SUV_{max} range 0.85–3.13, mean 1.62) uptake in the nodules to those in the control group. Three lesions of pneumonia in three cases showed similar or lower FDG [SUV_{max} range 0.67–2.73, mean 1.79 ± 0.60 (SE)] and MET [SUV_{max} range 0.80–2.03, mean 1.45 ± 0.36 (SE)] uptake in the nodules than those in the control group.

Discussion

Silicosis, coal worker pneumoconiosis, and asbestosis are the three most common types of pneumoconiosis, and are examples of fibrotic pneumoconiosis. Japanese coal miners were exposed to relatively high concentrations of silica dust [10], and therefore tend to suffer from silicosis [11, 12]. Progressive massive fibrosis (PMF) is frequently bilateral and also tends to be accompanied by widespread nodulation in the remainder of the lung, although sometimes the localization is not typical. It is

Table 3 Patient and tumor characteristics

No.	Size (cm)/location	Method of final diagnosis	Final diagnosis	SUV_{max}		PET diagnosis	
				MET	FDG	MET	FDG
1	3.0/C	TBB	SCC	5.81	11.76	TP	TP
2	0.7/P	Operation	AC	0.65	0.82	FN	FN
3	1.5/P	TBB	AC	2.01	4.05	TP	TP
4	2.0/P	Operation	SqCC	2.62	5.54	TP	TP
5	14.0/C	Needle biopsy	LCC	5.53	7.26	TP	FN

TBB transbronchial biopsy, *SCC* small cell carcinoma, *AC* adenocarcinoma, *SqCC* squamous cell carcinoma, *LCC* large cell carcinoma, *TP* true positive, *FN* false negative, *C* central type, *P* peripheral type

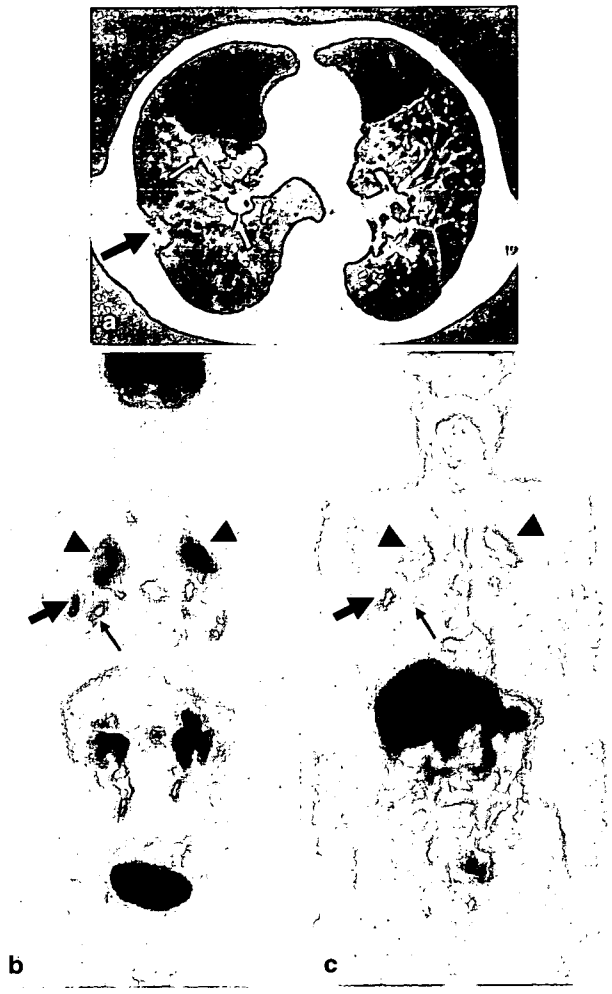

Fig. 4 Lung cancer and pneumoconiosis in a 77-year-old man who worked for 29 years in a coal mine. The CT scan (**a**) revealed a pleural-based increased 1.5-cm-long adenocarcinoma (*large arrow*) and 2.0 cm-long pneumoconiotic nodule (*small arrow*) in the right lung. FDG (**b**) and MET (**c**) accumulated in the malignant nodule more than in the pneumoconiotic nodule. SUV_{max} of FDG and MET in the lung cancer were 4.05 and 2.01, whereas those in the pneumoconiotic nodule were 3.28 and 1.35, respectively. Bilateral large pneumoconiotic nodules existed in upper lungs (*arrowhead*), similar to the findings in Fig. 1b

Fig. 5 Lung large cell carcinoma in large pneumoconiotic nodule in a 69-year-old man who worked for 41 years in a coal mine. Axial CT scan (**a**) shows a 14-cm-long nodule (*arrow*) in the right lung. FDG-PET image (**b**) shows very intense uptake in the large bulky nodule, whereas MET-PET image (**c**) demonstrates that the tumor exists mainly in lower lesion suspected malignancy of the large nodule. A small liver metastasis and a small metastasis in the lung (*arrowhead*) are visualized on FDG PET

clinically important and radiologically difficult to differentiate lung cancer from PMF.

Fluoro-deoxy-D-glucose is a known tracer of glycolysis, which is taken up and retained by cancer cells because of the presence of glucose transporters (glut-1) and so on [13, 14]. Kubota et al. [15] reported autoradiography studies to demonstrate a high accumulation of FDG in macrophages and young granulation tissue. Because pneumoconiotic nodules are composed of macrophages and granulomatous inflammation (as in tuberculous infection) [16], PMF often shows a significant increase in the FDG uptake related to the presence of inflammatory cells such as macrophages, as well as fibroblasts [17].

C-11-methionine has been used to measure amino acid metabolism in vivo, and a high MET uptake in tumor cells is thought to reflect an increase in either the transport mechanism of amino acids or the transmethylation pathway. The accumulation of MET in lung cancer has been reported to usually be lower than that of FDG [2]. In animal models, Kubota et al. [18] reported that MET distribution in tumor tissue was more specific for viable cancer cells compared with FDG. Granulation tissue and macrophages exhibited uptake of MET at levels lower than those of FDG. Tumor uptake of MET is predominantly by viable cancer cells. Zhao et al. [19] in our group recently suggested that the accumulation of

MET in the granuloma was significantly lower than that in the tumor.

Pneumoconiotic nodules are known to show persistent, fibrotic, and progressive inflammatory change, and both FDG and MET accumulate in the inflammatory cells in these nodules. We therefore hypothesized that the degree of accumulation of the two PET tracers in pneumoconiotic nodules may be size dependent. In a control group, a significant correlation between the nodular size and SUV_{max} of the two PET tracers was observed in pneumoconiosis. This preliminary study indicates that the degree of accumulation of MET was size dependent, as was that of FDG (Fig. 2). This study suggested that MET accumulated not only in malignant lesions but also in benign pneumoconiotic nodules, although the SUV_{max} of MET was significantly lower than that of FDG. We next attempted to differentiate and evaluate lung cancer on the basis of the degree of size-dependent accumulation in the pneumoconiotic nodules in the suspected lung cancer group. Three of the five cases showed high FDG and MET uptake relative to the size, and therefore, were properly diagnosed to have lung cancer both by FDG and MET-PET. The present study indicates that nodules with an intense uptake of both FDG and MET relative to their size should thus be carefully observed because of a high risk for lung cancer.

In pneumoconiosis, the incidence of lung carcinoma is reported to be 17.9%, with the most common type being squamous cell carcinoma (54.2%) followed by small cell carcinoma (22.9%), and adenocarcinoma [20]. For the discrimination of lung cancer from pneumoconiotic nodules, it is necessary to make judgments when taking the associated site into consideration, along with size and histological type. When the nodule develops at peripheral sites of the lungs, the existence of either peripheral-type squamous cell carcinoma or adenocarcinoma should be considered. In this case, discrimination appears to be possible, because the accumulation degree was found to be greater for lung cancer than for pneumoconiotic nodules. As for nodules those were equal to or less than 3cm in size, the regional tracer uptake (SUV_{max}) of FDG and MET in lung cancer were both significantly higher than in pneumoconiotic nodules (Fig. 3). However, it is difficult to evaluate very small well-differentiated adenocarcinomas in patients with normal lungs. As a result, such adenocarcinomas are around the detection limit also for patients with pneumoconiosis, as in this study. It is considered that squamous cell carcinoma and small cell carcinoma that developed in the center of the lungs can be evaluated via SUV_{max}, because both show a high degree of tracer accumulation. We were able to indicate the presence of malignancy in the case of 2-cm-long squamous cell carcinoma of the lung hilum with FDG-PET SUV_{max} of 11.76 and MET-PET SUV_{max} of 5.81.

When a nodule is very large, it is not as difficult to make a judgment regarding whether it is clinically malignant, using CT, magnetic resonance imaging, tumor markers, the existence of metastatic focus, and so on. On the basis of PET, the degree of FDG accumulation in the pneumoconiotic nodule becomes significantly greater to the extent that the accumulation in lung cancer cannot be differentiated from accumulation in the pneumoconiotic nodule. In this study, the difference in the accumulation between lung cancer and granulation may be better indicated with MET-PET rather than FDG-PET in large nodules (Fig. 2). There was one case showing intense uptake of FDG in a large bulky nodule but focal and high MET uptake in the lower portion of the large nodule suggesting lung cancer. On the basis of the criteria from the control group, lung cancer was highly suspected with MET-PET with a false-negative finding on FDG-PET (Fig. 5).

When we use MET alone to identify lung cancers, the degree of accumulation of MET in lung tumor, as well as lymph node metastasis, is usually lower than that of FDG, and thus the findings were not clear. In addition, the FDG-PET evaluation of metastasis and other malignant lesions would be better as compared with MET-PET. Therefore, we recommend the combined use of MET and FDG.

The major limitation of the present study is the limited number of patients, particularly, those with lung cancer among patients with pneumoconiosis. However, this preliminary study suggests that both FDG-PET and MET-PET may hold promise to differentiate lung cancer from benign pneumoconiotic nodules. FDG-PET has an advantage as metastasis and other associated malignant tumors can be detected as well. On the other hand, when the nodule is large, MET-PET may provide more morphological information than FDG-PET. A prospective study is currently underway to collect more patient data to support the additional value of MET-PET in conjunction with FDG-PET for the diagnosis of lung cancer developing in pneumoconiosis patients.

In conclusion, lung cancer is highly suspected in the presence of high FDG or MET uptake relative to the size of a lesion in patients with pneumoconiosis. MET-PET may be involved in identifying lung cancer in these patients in conjunction with FDG-PET.

References

1. Lewis PJ, Salama A. Uptake of fluorine-18-fluorodeoxyglucose in sarcoidosis. J Nucl Med 1994;35:1647–9.

2. Sasaki M, Kuwabara Y, Yoshida T, Nakagawa M, Koga H, Hayashi K, et al. Comparison of MET-PET and FDG-PET for differentiation between benign lesions and malignant tumors of the lung. Ann Nucl Med 2001;15:425–1.
3. Yamada Y, Uchida Y, Tatsumi K, Yamaguchi T, Kimura H, Kitahara H, et al. Fluorine-18-fluorodeoxyglucose and carbon-11-methionine evaluation of lymphadenopathy in sarcoidosis. J Nucl Med 1998;39:1160–6.
4. Knopp MV, Bischoff HG. Evaluation of pulmonary lesions with positron emission tomography. Radiologe 1994;34: 588–91.
5. Bakheet S, Powe J. 18-FDG uptake due to benign pathology. Semin Nucl Med 1998;28:352–8.
6. Strauss L. Fluorine-18 deoxyglucose and false-positive results: a major problem in the diagnostics of oncological patients. Eur J Nucl Med 1996;23:1409–15.
7. Kubota K, Matsuzawa T, Ito M, Ito K, Fujiwara T, Abe Y, et al. Lung tumor imaging by positron emission tomography using C-11 L-methionine. J Nucl Med 1985;26:37–42.
8. Yamamoto F, Tsukamoto E, Nakada K, Takei T, Zhao S, Asaka M, et al. 18F-FDG PET is superior to 67Ga SPECT in the staging of non-Hodgkin's lymphoma. Ann Nucl Med 2004;18:519–26.
9. Ramos CD, Erdi YE, Gonen M, Riedel E, Yeung HW, Macapinlac HA, et al. FDG-PET standardized uptake values in normal anatomical structures using iterative reconstruction segmented attenuation correction and filtered back-projection. Eur J Nucl Med 2001;28:155–64.
10. Ishinishi S. Silicosis. Fukuoka Acta Med 1956;47:926–30.
11. Tanaka S, Naruo Y, Toyofuku T. Silicosis and silicotuberuculosis in a coalmine. Jpn J Ind Med 1960;2:622–8.
12. Une H, Esaki H, Osajima K, Ikui H, Kodama K, Hatada K. A prospective study on mortality among Japanese coal miners. Ind Health 1995;33:67–76.
13. Mochizuki T, Tsukamoto E, Kuge Y, Kanegae K, Zhao S, Hikosaka K, et al. FDG uptake and glucose transporter subtype expressions in experimental tumor and inflammation models. J Nucl Med 2001;42:1551–5.
14. Zhao S, Kuge Y, Mochizuki T, Takahashi T, Nakada K, Sato M, et al. Biologic correlates of intratumoral heterogeneity in 18F-FDG distribution with regional expression of glucose transporters and hexokinase-II in experimental tumor. J Nucl Med 2005;46:675–82.
15. Kubota R, Yamada S, Kubota K, Ishiwata K, Tamahashi N, Ido T. Intratumoral distribution of fluorine-18-fluorodeoxyglucose in vivo: high accumulation in macrophages and granulation tissue studied by microautoradiography. J Nucl Med 1992;33:1972–80.
16. International Labour Organization. Fourth International Pneumoconiosis Conference: report of the working party on the definition of pneumoconiosis. Geneva, Switzerland: International Labour Organization; 1971.
17. Alavi A, Gupta N, Alberini JL, Hickeson M, Adam LE, Bhargava P, et al. Positron emission tomography imaging in nonmalignant thoracic disorders. Semin Nucl Med 2002;32: 293–321.
18. Kubota R, Kubota K, Yamada S, Tada M, Takahashi T, Iwata R, et al. Methionine uptake by tumor tissue: a microautoradiographic comparison with FDG. J Nucl Med 1995;36:484–92.
19. Zhao S, Kuge Y, Nakada K, Takei T, Kohanawa M, Zhao Y, et al. ^{11}C-methionine but not ^{18}F-FDG and ^{18}F-FLT can differentiate tumor from granuloma in experimental rat models [meeting abstract]. J Nucl Med 2006;47 Suppl 1:177P.
20. Ebihara I. A pathological study of carcinoma of the lung and pneumoconiosis. Jpn J Thorac Dis 1989;27:609–15.

A novel and efficient synthesis of [2-^{11}C]5-fluorouracil for prognosis of cancer chemotherapy

Koh-ichi Seki [1], Ken-ichi Nishijima [2], Yuji Kuge [3], Nagara Tamaki [3], Leonard I. Wiebe [4], and Kazue Ohkura [2]

[1] Central Institute of Radio Isotope Science, Hokkaido University, Sapporo, Japan; [2] Faculty of Pharmaceutical Sciences, Health Sciences University of Hokkaido, Hokkaido, Japan; [3] Graduate School of Medicine, Hokkaido University, Sapporo, Japan; [4] Faculty of Pharmacy & Pharmaceutical Sciences, University of Alberta, and Cross Cancer Institute, Edmonton, Alberta, Canada

In memory of Professor Antoine (Tony) A. Noujaim, whose outstanding contributions to radiopharmacy, diagnostic oncology and the immunotherapy of cancer will serve as an inspiration to us all.

Received January 2, 2007; Revision received January 15, 2007; Accepted January 15, 2007, Published June 14th 2007

ABSTRACT - Purpose: In order to facilitate the use of the PET-based 'Strauss test' for 5-FU sensitivity, a rapid and facile synthesis of [2-^{11}C]5-fluorouracil ([2-^{11}C]5-FU), based on [^{11}C]phosgene ([^{11}C]$COCl_2$), is reported. **Methods:** The key intermediate (*E*)-β-benzoylamino-α-fluoroacrylamide (**1**) and [^{11}C]phosgene was submitted to cyclo-condensation to give [2-^{11}C]5-fluorouracil. **Results:** [2-^{11}C]5-Fluorouracil was synthesized in 17 min with high (~25%) radiochemical yield. **Conclusion:** The present study provides a rapid, simple, and efficient synthesis of [2-^{11}C]5-FU, that would serve as a useful prognostic PET tracer for 5-FU chemotherapy.

INTRODUCTION

The original synthesis of 5-fluorouracil (5-FU), one of a new class of antitumor fluoroprymidines, was reported in 1957 (1,2). 5-FU-mediated inhibition of thymidylate synthetase (3) was subsequently shown to be one of the major mechanisms responsible for the antitumor activity of these compounds. Detailed studies have pointed to 5-FU interference with DNA and protein synthesis, as a result of conversion to the corresponding ribose nucleoside and substitution into RNA, as an equally important mechanism of toxicity (4). The first clinical studies of 5-FU were reported in 1958 (5). Radiolabeled 5-FU ([2-^{14}C]5-FU) (6) and [6-^{14}C]5-FU (7) have been used for biodistribution studies in animals and [2-^{14}C]5-FU biodistribution has been studied in cancer patients (8).

Today, almost 50 years later, 5-FU remains front-line therapy, alone or in combination with other drugs or radiation, for gastric (9,10), colorectal (11,12) and other cancers including advanced pancreatic cancer (13). In light of the limited success of cancer chemotherapy in general, including 5-FU, it is surprising that the medical community has not demanded, and relied upon, a rational basis for the prediction of more successful outcomes when selecting a chemotherapeutic drug. It has been demonstrated, for example, that tumor uptake of fluorine-18 labeled 5-FU ([^{18}F]5-FU) serves a positive prognostic role in selection of patients for 5-FU therapy (Strauss [^{18}F]5-FU test) (14, 15). Under-utilization of the 'Strauss [^{18}F]5-FU test' may be due, in part, to the proposed need for complex kinetic modeling rather than simple tumor uptake (16), and/or to the electrophilic F-18 radiosynthetic method developed in the early 1970's [17]. The latter method remains the sole method of 5-FU radiosynthesis today, and is thus not popular in units using the ^{18}O(p,n)^{18}F nuclear reaction to produce aqueous radiofluoride for routine clinical radiofluorinations. The ease of use of the latter approach has resulted in a largely 'nucleophilic' F-18 labeling world.

Since only F, N, O, H and C can be used to radiolabel 5-FU without altering its biochemistry, F-18 and C-11 offer the only opportunity for nuclear (positron emission tomographic; PET) imaging. Pyrimidine nucleosides have been labeled with C-11 at C-2 (18,19), and PET studies using C-11 nucleosides have been reported (20), but [2-^{11}C]5-FU is not among those reported. In order to facilitate the use of the PET-based 'Strauss test' for 5-FU sensitivity, a rapid, facile synthesis of [2-^{11}C]5-fluorouracil ([2-^{11}C]5-FU), based on [^{11}C]phosgene ([^{11}C]$COCl_2$) (21), has been developed and is now reported (Figure 1).

Corresponding author: Koh-ichi Seki, Ph. D, Central Institute of Radio Isotope Science, Hokkaido University, Kita-15, Nishi-7, Kita-ku, Sapporo Tel: +81-11-706-6090, E-mail: seki@ric.hokudai.ac.jp

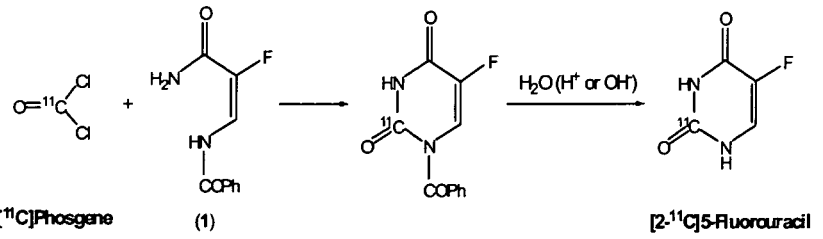

Figure 1. Synthetic route for [2-^{11}C]5-fluorouracil.

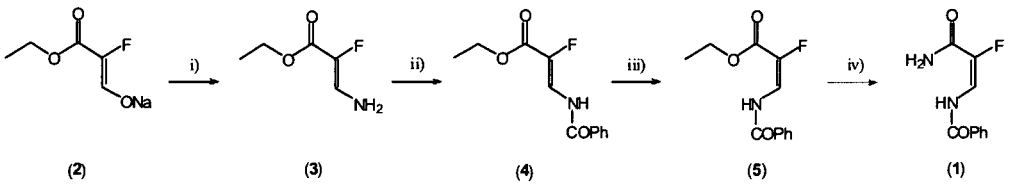

Reagents and Conditions :
i) NH_4Cl-CH_3OH, NH_3, 4 days, ii) $PhCOCl$, C_5H_5N, ether, overnight, iii) hn (h.p.-Hg-lamp), iv) NH_3, CH_3OH, 1 week

Figure 2: Synthesis of the 5-fluorouracil precursor (1).

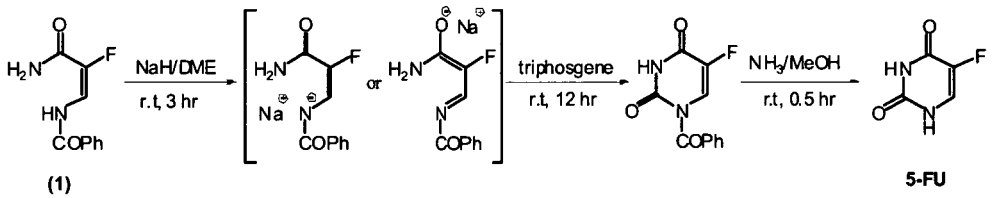

Figure 3. Synthesis of 5-fluorouracil (5-FU).

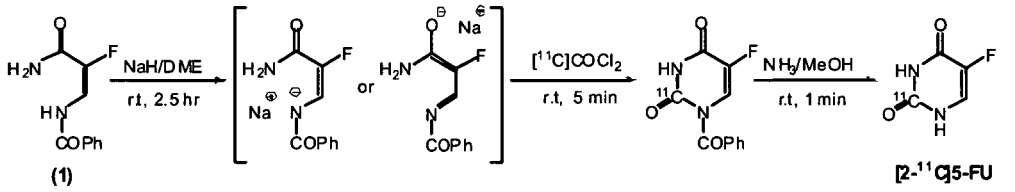

Figure 4. Synthesis of [2-^{11}C]5-FU.

MATERIALS AND METHODS

Chemicals

Triphosgene was purchased from Aldrich Chemical Co. Ltd. (St. Louis, MO). All solvents were reagent grade and distilled using the appropriate methods. [^{11}C]$COCl_2$ was synthesized from [^{11}C]CH_4 *via* [^{11}C]CCl_4 according to our previously reported method [21]. Bombardment was carried out with a 10 μA beam of 18 MeV protons for 10 min. The yield of [^{11}C]$COCl_2$ was estimated to be about 1500 MBq based on the yield of [^{11}C]diphenylurea produced with aniline under the same conditions.

RESULTS

Synthesis of (E)-β-benzoylamino-α-fluoroacrylic amide (1)

Our first goal was the synthesis of the key intermediate **1**, which would undergo cyclocondensation with [^{11}C]phosgene at the final step into [2-^{11}C]5-FU: Treatment of ethyl 2-fluoro-3-hydoxyacrylate sodium salt (**2**) [22] with ammonia (NH_3) and ammonium chloride in methanol gave rise to the formation of β-aminoacrylate (**3**) [23]. Benzoylation of the resulting **3** with benzoyl chloride in pyridine afforded (*Z*)-ethyl β-benzoyl-amino-α-fluoroacrylate (**4**), wherein the ethoxy-carbonyl group and the benzoylamino group occupy the *trans*-stereochemistry on the ethylene moiety. In order to effect geometric isomerization of the *Z*-isomer **4** into the *E*-isomer **5**, **4** was irradiated with a high-pressure mercury lamp, to afford the equilibrium mixture of **5** and **4** in the ratio of 1: 9. The *E*-isomer **5**, having a convenient stereochemistry for the ring closure with phosgene, was further treated with NH_3, resulting in the production of the key intermediate **1** in quantitative yield with the desired stereochemistry (*E*-form) (Figure 2).

Synthesis of cold 5-FU

The sodium salt of the key intermediate **1** was subjected to cyclocondensation with triphosgene at room temperature, followed by the hydrolysis with 2 M NH_3 in methanol, resulting in the formation of 5-FU in high yield (75%, after purification on HPLC) (Figure 3).

Synthesis of [2-^{11}C]5-FU

The key intermediate **1**, activated as the sodium salt, was subjected to cyclocondensation with [^{11}C]$COCl_2$ (23) on the same automated synthesis system used for the production of *S*-[^{11}C]CGP-12177 (24). The total synthesis took 17 minutes from the end of bombardment to isolation of [2-^{11}C]5-FU. The yield of [2-^{11}C]5-FU was 380 MBq at EOS (Figure 4). The radiochemical yield of [2-^{11}C]5-FU was approximately 25%. The radio-HPLC trace is shown in Figure 5.

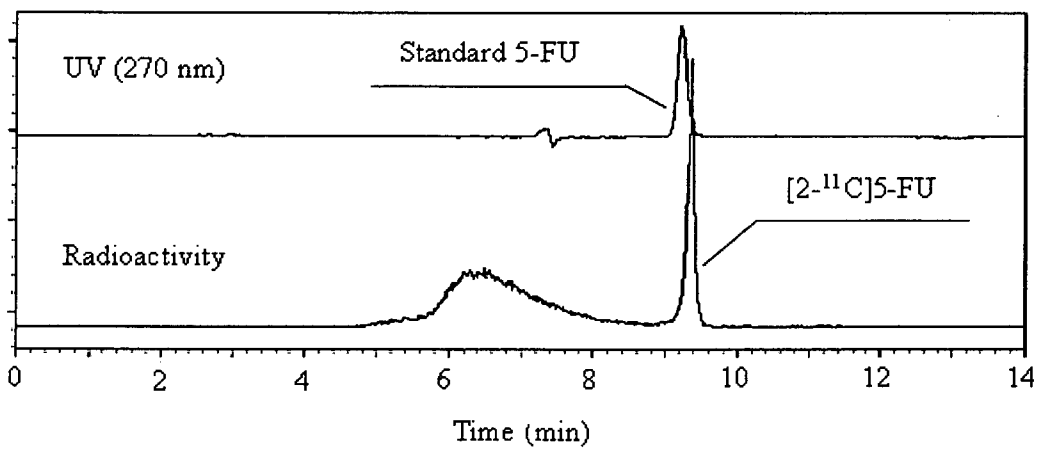

Figure 5. Chromatographic data for the analysis of [2-^{11} C]5-FU. [2-^{11}C]5-FU was analyzed by reverse-phase HPLC (Inertsil ODS-3, 250 mm x 4.6 mm *i.d.*) with elution of 3% ethanol in water at a flow rate of 0.5 mL/min. The chromatogram was monitored continuously based on radioactivity (RLC-700, Aloka, Tokyo, Japan) and absorbance at 270 nm (SPD-10 Avp, Shimadzu).

DISCUSSION

[2-^{11}C]5-FU was synthesized by the cyclocondensation of newly developed (*E*)-β-benzoylamino-α-fluoroacrylic amide (1) with [^{11}C]$COCl_2$. The success in the synthesis lies in the synthesis of the key intermediate **1** bearing proper stereochemistry, and on the application of highly reactive species [^{11}C]$COCl_2$ for cyclocondensation in the final step. These radiochemical yields (25%) compare favorably with yields (23%) reported previously for the synthesis of [2-^{11}C]thymine using [^{11}C]COCl2 (23). Importantly, the radiochemical yields are adequate for in vivo studies of [2-^{11}C]5-FU uptake in patients, and would appear sufficient for analysis of 1-h time-activity curves (20)using the catenary, three-compartment, five-parameter model developed for 5-[^{18}F]FU in vivo (16).

CONCLUSION

The present study demonstrates the first efficient synthesis of [2-^{11}C]5-FU, which would be a useful PET-tracer for the assessment and prediction of outcomes of 5-FU in chemotherapeutic treatment.

ACKNOWLEDMENT

This work was in part supported by a Grant-in-Aid from the Ministry of Education, Culture, Sports, Science and Technology of Japan.

REFERNCES

[1] Heidelberger, C., Chaudhuri, N.K., Danneberg, P., Mooren, D., Griesbach, L., Duschinsky, R., Schnitzer, R.J., Pleven, E., Scheiner, J. Fluorinated pyrimidines, A new class of tumour-inhibitory compounds. Nature, 179: 663-666, 1957.

[2] Duschinsky, R., Pleven, E., Heidelberger, C. The synthesis of 5-fluoropyrimidines. J. Am. Chem. Soc., 79: 4559, 1957.

[3] Hartmann, K.U., Heidelberger C. Studies on fluorinated pyrimidines. XII. Inhibition of thymidylate synthetase. J. Biol. Chem., 236: 3006, 1961.

[4] Myers, C.E. The pharmacology of the fluoropyrimidines. Pharmacological Reviews, 33: 1-15, 1981.

[5] Curreri, A.R., Ansfield , F.J., McIver, F.A., Waisman, H.A., Heidelberger, C. Clinical studies with 5-fluorouracil. Cancer Res, 18: 478-484, 1958.

[6] Chaudhuri, N.K., Montag, B., Heidelberger, C. Studies on fluoropyrimidines. XVI. Metabolism of 5-fluorouracil-2-^{14}C and 5-fluoroorotic-2-^{14}C acid in vivo. Cancer Res., 18: 318-328, 1958.

[7] Mukherjee, K.L., Heidelberger, C. Studies on fluorinated pyrimidines. IX. The degradation of 5-fluorouracil-6-^{14}C. J. Biol. Chem., 235: 433-7, 1960.

[8] Mukherjee, K.L., Curreri, A.R., Jauid, M. Heidelberger, C. Tissue distribution of 5-fluorouracil-2-^{14}C and 5-fluoro-2'-deoxyuridine in cancer patients. Cancer Res., 23: 67, 1963.

[9] Tahara, M., Ohtsu, A., Boku, N., Nagashima, F., Muto, M., Sano, Y., Yoshida, M., Mera, K., Hironaka, S., Tajiri, H., Yoshida, S. Sequential methotrexate and 5-fluorouracil therapy for gastric cancer patients with peritoneal dissemination: a retrospective study. Gastric Cancer, 4: 212-218, 2001.

[10] Van Cutsem, E., Moiseyenko, V.M., Tjulandin, S., Majlis, A., Constenla, M., Boni, C., Rodigues, A., Fodor, M., Chao, Y., Voznyi, E., Risse, M.L., Ajani, J.A. Phase III study of docetaxel and cisplatin plus fluorouracil compared with cisplatin and fluorouracil as first-line therapy for advanced gastric cancer: a report of the V325 Study Group. J. Clin. Oncol., 24: 4991-4997, 2006.

[11] Patiyil, S., Alberts, S.R. Metastatic colorectal cancer: Therapeutic options. Curr. Treat. Options Oncol., 7: 389-398, 2006.

[12] Goyle, S., Maraveyas, A. Chemotherapy for colorectal cancer. Dig. Surg., 22: 401-414, 2005.

[13] Park, J.K., Ryu, J.K., Lee, J.K., Yoon, W.J., Lee, S.H., Kim, Y.T., Yoon, Y.B. Gemcitabine chemotherapy versus 5-fluorouracil-based concurrent chemoradiotherapy in locally advanced unresectable pancreatic cancer. Pancreas, 33: 397-402, 2006.

[14] Dimitrakopoulou-Strauss, A., Strauss, L.G., Schlag, P., Hohenberger, P., Irngartinger, G., Oberdoorfer, F., Doll, J., Van Kaick, G. Intravenous and intra-arterial oxygen-15-labeled water and fluorine-18-labeled fluorouracil in patients with liver metastases from colorectal carcinoma. J. Nucl. Med., 39: 465-473, 1998.

[15] Kissel, J., Brix, G., Bellemann, M.E., Strauss, L.G., Dimitrakopoulou-Strauss, A., Port, R., Haberkorn, U., Lorenz, W.J. Pharmacokinetic analysis of 5-[^{18}F]fluorouracil tissue concentrations measured with positron emission tomography in patients with liver metastases from colorectal adenocarcinoma. Cancer Res., 57: 3415-3423, 1997.

[16] Bading, J.R., Yoo, P.B., Fissekis, J.D., Alauddin, M.M., D'Argenio, D.Z., Conti, P.S. Kinetic modeling of 5-fluorouracil anabolism in colorectal adenocarcinoma: a positron emission tomography study in rats. Cancer Res., 63: 3667-3674, 2003.

[17] Fowler, J.S., Finn, R.D., Lambrecht, R.M., Wolf, A.P. The synthesis of ^{18}F-5-fluorouracil. VII. J. Nucl. Med., 14: 63-64, 1973.

[18] Sundoro-Wu, B.M., Schmall, B., Conti, P.S., Dahl, J.R., Drumm, P., Jacobsen, J.K. Selective alkylation of pyrimidyldianions: synthesis and purification of ^{11}C labeled thymidine for tumor visualization using positron emission tomography. Int. J. Appl. Radiat. Isot., 35: 705-708, 1984.

[19] Link, J.M., Grierson, J., Krohn, K. Alternatives in the synthesis of 2-[C-11]thymidine. J. Labelled Compd. Radiopharm., 37: 610-612, 1995.

[20] Mankoff, D.A., Shields, A.F., Graham, M.M., Link, J.M., Eary, J.F., Krohn, K.A. Kinetic analysis of 2-[carbon-11]thymidine PET imaging studies: compartmental model and mathematical analysis. J. Nucl. Med., 39: 1043-1055, 1998.

[21] Nishijima, K., Kuge, Y., Seki, K., Ohkura, K., Motoki, N., Nagatsu, K., Tanaka, A., Tsukamoto, E., Tamaki, N. A simplified and improved synthesis of [^{11}C]phosgene with iron and iron (III) oxide. Nucl. Med. Biol., 29: 345-350, 2002.

[22] Miyamoto, T., Egawa, H., Matsumoto, J. Pyridonecarboxylic acids as antibacterial agents. VIII. An alternative synthesis of enoxacin via fluoronicotinic acid derivatives. Chem. Pharm. Bull., 35: 2280-2285, 1987.

[23] Ohkura, K., Nishijima, K., Sanoki, K., Kuge, Y., Tamaki, N., Seki, K. A new convenient method for the synthesis of [2-^{11}C]thymine utilizing [2-^{11}C]phosgene. Tetrahedron Lett., 47: 5321-5626, 2006.

[24] Nishijima, K., Kuge, Y., Seki, K., Ohkura, K., Morita, K., Nakada, K., Tamaki, N. Preparation and pharmaceutical evaluation for clinical application of high specific activity S-(-)[^{11}C]CGP-12177, a radioligand for β-adrenoreceptors. Nucl. Med. Commun., 25: 845-849, 2004.